Microfluidics

DOI: 10.1002/anie.200800816

Microfluidic Self-Patterning of Large-Scale Crystalline Nanoarrays for High-Throughput Continuous DNA Fractionation**

*Yong Zeng, Mei He, and D. Jed Harrison**

Self-assembly offers an attractive route to produce macroscopic functional ensembles from microscopic building blocks, such as macromolecules, colloids, and nanotubes.[1,2] Spontaneous organization of monodispersed colloids into crystalline arrays, dubbed colloidal self assembly (CSA), has been extensively explored in a variety of areas, such as the design of materials,[3] photonics,[4] sensors,[5] and molecular manipulation and separation.[6–10] High quality colloidal films with minimal lattice defects and large domain size have been achieved.[11,12] Success in many applications will also demand the ability to pattern self-assembled colloidal lattices into well-defined architectures and within integrated microsystems. A number of patterning methods have been developed, including physical confinement,[13–15] electric field-assisted patterning,[16] and surface-directed patterning.[17] Large-scale colloidal patterning, however, still suffers from long processing time and major defects, particularly cracks. Herein, we report a microfluidic approach for patterning large-area colloidal arrays into complex microdevices, which controls evaporation-induced colloidal crystallization to avoid the formation of cracks.

To exemplify the application of this technique, a patterned large-area colloidal nanoarray was demonstrated as molecular sorting structure for continuous separation of DNA. Its counterparts, lithographically fabricated micro-/nanostructures have been widely used for bioseparations.[18–21] However, their practical applications are largely impeded by current technical limitations of nanolithography, such as high cost, tedious fabrication, and challenges in fabrication at 10 nm length scales. In this regard, CSA provides a simple and cost-effective alternative, especially for large-area patterning of nanoscale features. For instance, compared to two-dimensional (2D) microfabricated post arrays,[19,20] our device demands much less effort and cost of fabrication; it possesses a 3D periodic porous structure, which eases operation and improves sample throughput; and it offers great flexibility in varying pore size to target certain molecular size ranges.

Preparation of large crack-free colloidal structures are much more challenging than assembling narrow 1D bands by a single-channel CSA approach,[7] due to the heterogeneous capillary stress built across a large area during solvent evaporation. CSA in slab fluidic cells commonly used for growing large-area colloidal films generates a pattern of cracks which are spaced periodically along the evaporating edge and propagate parallel from the end into the bulk.[22,23] Capillary stress was found to be the driving force for film fracturing and the spatial period of cracks was thought to be set by the characteristic length of stress variation along the drying edge, which reflects the balance between evaporation-induced capillary pressure and stress relaxation by crack opening.[23,24] Our microfluidic self-patterning approach, illustrated in Figure 1a, uses multiple microchannels to guide CSA within large-scale microdevices. The microchannels reduce the stress nonuniformity by dividing wide open edges into segments shorter than the characteristic length scale above which cracking occurs, and prevent the drying front from penetrating into the bulk.[7]

Figure 1b presents the design of a 2D DNA sorting microdevice based on this methodology. It consists of a $4 \times 4\ mm^2$ square chamber connected to the reservoirs via 20 microchannels (100 μm × 5 mm, 200 μm periodicity) on each side. The microchannel arrays were designed by considering both experimental measurements of crack spacing in the literature[24,25] and the generation of fairly uniform electric fields over the large chamber.[26] Figure 1c shows that a PDMS device packed with 0.9 μm silica beads exhibits a spectrum of iridescent colors under white light illumination, due to Bragg scattering from the 3D periodic lattice. In Figure 1d, an as-prepared 330 nm silica nanoarray shows a uniformly translucent pattern, indicating the presence of interstitial water and no cracks formed. SEM imaging confirms the long-rang crystalline structure of close-packed 330 nm spheres, with the (111) plane parallel to the substrate (Figure 1e). A low density of lattice defects was also seen, which may affect the separation performance; but they are randomly distributed so that no accumulative effects like flow channeling will arise. Large-area colloidal arrays allow us to measure their optical properties as seen in Figure 1e. The characteristic stop band at $\lambda_{max} = 615$ nm corresponds to the first-order Bragg diffraction from a dried 330 nm silica nanoarray. The small deviation of λ_{max} between the freshly prepared nanoarrays ($\lambda_{max} = 613.0 \pm 2.8$ nm, $n = 5$) and those previously used for separations ($\lambda_{max} = 617.0 \pm 5.6$ nm, $n = 4$) implies fairly good stability of self-patterned nanoarrays under applied pulsing electric fields up to $170\ V\,cm^{-1}$. The whole device can be packed within less than 6 hrs for 10 % w/v 330 nm beads under ambient conditions, which is much faster than the approaches using sedimentation[9] and barrier structure.[14]

[*] Y. Zeng, M. He, Prof. D. J. Harrison
Department of Chemistry, University of Alberta
Edmonton AB, T6G 2G2 (Canada)
Fax: (+1) 780-492-8231
E-mail: jed.harrison@ualberta.ca

[**] This work was supported by the Natural Sciences and Engineering Research Council of Canada (NSERC). Microfabrication in this work was done at Nanofab, University of Alberta.

Supporting information for this article is available on the WWW under http://dx.doi.org/10.1002/anie.200800816.

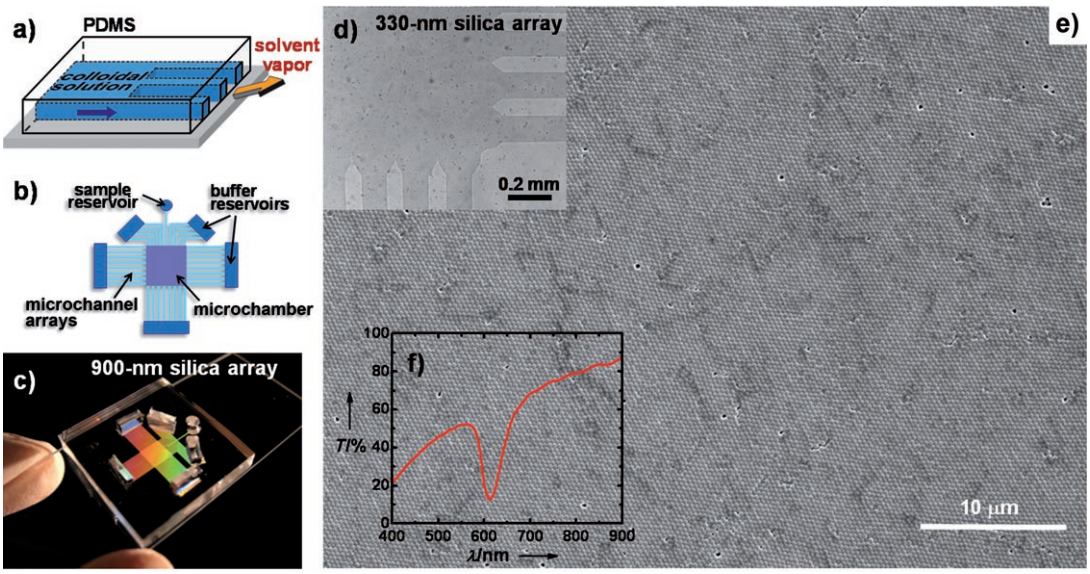

Figure 1. Microfluidic patterning of large crack-free colloidal crystalline arrays. a) Schematic of using multiple evaporation channels to assemble large-area colloidal arrays within complex microdevices. b) Design of a 2D DNA microfractionator based on self-assembled crystalline arrays. c) A PDMS chip packed with 0.9 μm silica spheres shows Bragg diffraction of light. d) Transmission micrograph of an as-prepared 300 nm silica array. e) SEM image and f) normal incidence transmission spectrum of large-area 330 nm silica arrays.

Continuous-flow separation under asymmetric pulsed fields is based on the biased reorientation mechanism, where DNA fragments can be separated into individual flow streams of different deflection angles, θ, as detailed in Figure 2a and b.[19] In our case, all separations were performed using 330 nm nanoarrays, unless otherwise mentioned, and ca. 135° pulsed fields ($E_1 \approx 1.4\,E_2$) applied across the separation beds. A clear separation of four DNA fragments of 2–20 kbp is seen in Figure 2c, showing smooth DNA streams with no flow channeling due to cracks. Figure 2d images selective separation of the largest 20-kbp fragment from a mixture by tuning the frequency from 2 to 4 Hz at $E_1 = 168\ \mathrm{V\,cm^{-1}}$. Smaller fragments can be well separated at $f = 15$ Hz with the resolution R_s higher than 2.0. Such improvement comes at the cost of resolution for the largest two fragments, because 20-kbp DNA seems to reach its maximum deflection.

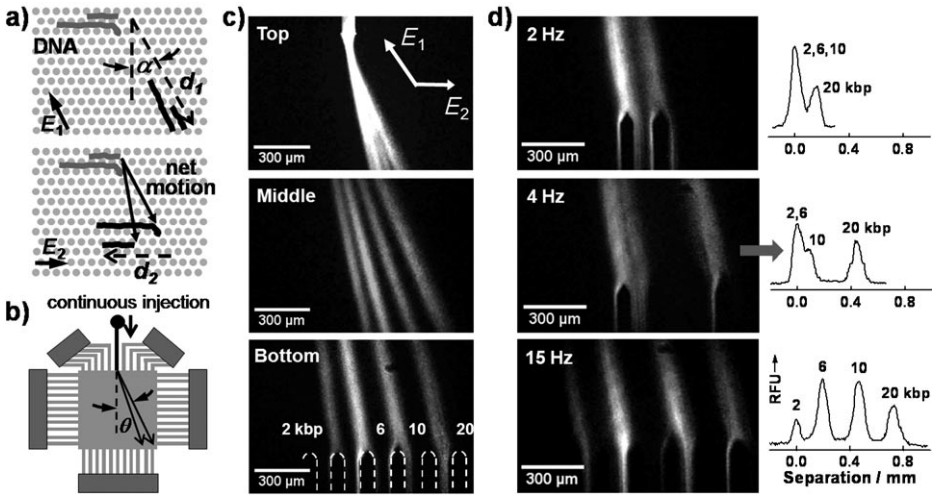

Figure 2. Continuous DNA fractionation. a) Schematic of biased reorientation mechanism under asymmetric pulsed fields ($E_1 > E_2$). Stretched DNA chains migrate a distance (d_1) against E_1. As E_2 is switched on, they reorient at different spots according to length and back track a distance (d_2), led by their previous trailing ends. Thus, they are differentiated in directions of net motion: the larger chain is more deflected from the average field direction than the small one. α is the angle of vector d_2 relative to the normal. b) Continuous-flow separation of DNA. θ is defined as the deflection angle between a DNA stream and the normal. c) Fluorescence images of fractionating 2–20 kbp DNA in a 330 nm silica array ($E_1 = 112\ \mathrm{V\,cm^{-1}}$, $f = 10$ Hz) taken from the top, middle, and bottom of the chamber, respectively. The collecting channels in the bottom frame were outlined for clarity. d) DNA separations at various frequencies ($E_1 = 168\ \mathrm{V\,cm^{-1}}$). The intensity profiles (right) were obtained from the fluorescent images (left) by scanning right above the collecting channels (as indicated by the gray arrow), with the center of 2-kbp peak (or co-migrating peak) defined as the origin of the horizontal axis.

Huang et al. also observed the field dependency of angular DNA separation in a "DNA prism" microdevice.[19] However, there is a lack of clear studies on how the conditions and separations are correlated. Our systematical investigation clearly depict a peaking response of DNA deflection angle to frequency and a characteristic size dependency of the maximum deflection angle, which have not been reported previously. Figure 3a–c shows that, as the frequency increases, the deflection angles arise from a lower plateau to a maximum

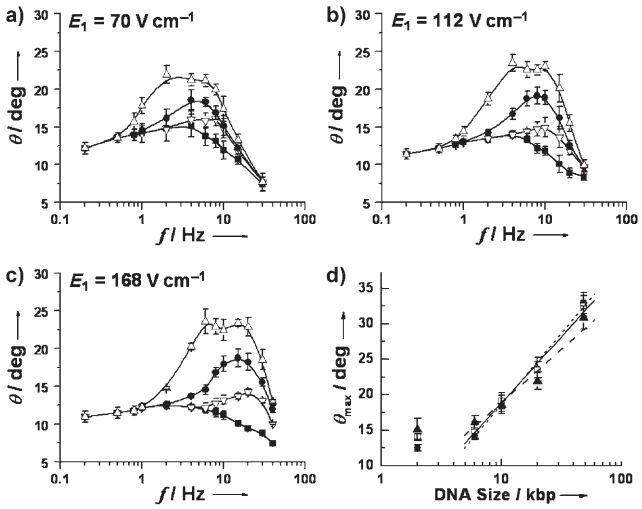

Figure 3. Effects of pulsed field on DNA deflection. a–c) Frequency spectra of deflection angle θ for various DNA fragments (△: 20 kbp, ●: 10 kbp, ▽: 6 kbp, ■: 2 kbp) under different field strength. Angles were measured from the middle of the separation chamber to minimize the effect of field distortion. Lines are drawn to guide eyes. d) Semilog plot of θ_{max} against DNA molecular weight with least-squares linear fit. Error bars show standard deviations ($n=3$). ▲: $E_1=70$ V cm^{-1}, □: $E_1=112$ V cm^{-1}, ●: $E_1=168$ V cm^{-1}.

according to DNA sizes, leading to the size and frequency dependent separation of four DNA fragments. This is consistent with the simple model, drawn in Figure 2a, which considers a DNA chain as a flexible rod of a constant extension (see Supporting Information for the discussion).

A striking feature is the size dependency of θ_{max}. Figure 3d plots θ_{max} against DNA size, which clearly manifests that θ_{max} is a characteristic measure of the size for DNA of 6–48 kbp. This observation is contrary to the prediction of the deterministic model of constant DNA length, that is, $\theta_{max} \approx 45°$, regardless of size, which implies that molecular dynamics of DNA electrophoresis significantly affects the deflection behavior. We propose that the stochastic fluctuation of DNA length should play an important role in the size dependency of θ_{max}.[27] Assume that a DNA chain reaches the maximum deflection at a given frequency, that is, its extension $l=d_2$. In a cycle with positive fluctuation superimposed on its length at the end of pulse E_2 ($l+\Delta l > d_2$), the chain cannot complete the reorientation by E_2 and still drifts along the stronger field E_1. But a negative fluctuation ($l-\Delta l < d_2$) in another cycle allows it to backtrack completely away from the sliding point at the end of pulse E_2, causing less deflection. After many cycles, the molecule follows an average θ_{max} that is smaller than α, the upper limit set by the field E_1. Therefore, θ_{max} reflects the extent of fluctuation of DNA chains.

The longitudinal fluctuation-in-a-tube model developed for pulsed-field gel electrophoresis proposes that the averaged relative fluctuation scales with molecular size, N, by $\Delta l/l \sim 1/\sqrt{N}$.[27] This scaling predicts smaller relative fluctuation for larger DNA, qualitatively consistent with Figure 3d. Single-molecule imaging of λ-DNA displays the length fluctuation and conformation changes during their episodic motion in the maximum deflection regime (Supporting Information, Movie 1). The precise understanding of the size dependency of θ_{max} requires quantitative analysis and numerical simulation to capture the transient dynamics of DNA molecules. Such an analysis is crucial for studying the size selectivity and band dispersion of the angular separation in colloidal arrays.

The deflection angle decreases with increasing f after the maximum deflection, and DNA chains were observed to drift at slow speeds, contrary to a dynamic trapping regime that the simplified model pictures (Supporting Information). It was seen that DNA chains developed random hernias at high frequencies, so that the molecule is poorly oriented with either field vector (Supporting Information, Movie 2). In effect, this suppresses the ratchet effect of asymmetric pulsed fields, which could account for the decrease of deflection angles.

The 2-kbp DNA responds differently to frequency than larger DNA and its θ_{max} deviates qualitatively from the trend for others (Figure 3), implying a change of separation mechanism. The contour length of a 2-kbp dsDNA is ca. 680 nm, spanning only two 330 nm spheres. Taking into account the partial extension and fast relaxation of short DNA, it is more likely for 2-kbp DNA to reptate along a zigzag path,[27,28] in contrast to the characteristic chevron pattern in the reorientation mechanism. This indicates the effect of lattice dimension on the lower size limit of efficient separation. Figure 3d suggests the mechanism transition occurs near 6 kbp in this 330 nm colloidal array.

To evaluate the effect of field strength on separation resolution, we compared the separations at various field strengths that yield the highest peak capacities $n_{c,max}$ between 2 and 20 kbp (Figure 3). We determined $n_{c,max}=4$ at $f=6$ Hz for $E_1=70$ V cm^{-1}, $n_{c,max}=7$ at $f=10$ Hz for $E_1=112$ V cm^{-1}, and $n_{c,max}=8$ at $f=15$ Hz for $E_1=168$ V cm^{-1}. Those values were plotted in Figure 4a, which shows that better separation can be achieved under higher field strength and that the improvement is mainly in the range of 2–10 kbp. This could be attributed to the size dependency of DNA electrophoretic stretching.[29,30] High field strength is desired for better stretching of short DNA, and the corresponding high frequency favors the separation of short DNA as well, by

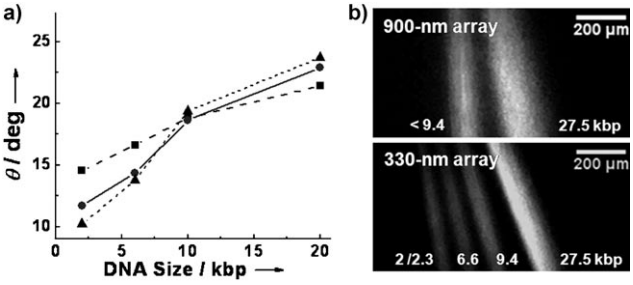

Figure 4. Effects of pulsed field and pore size on separation resolution. a) Plots of θ obtained in three separations as a function of molecular weight. For each field strength, frequency was chosen to give the highest peak capacity between 2 and 20 kbp. ■: $E_1=70$ V cm^{-1}, $f=6$ Hz; ●: $E_1=112$ V cm^{-1}, $f=10$ Hz; ▲: $E_1=168$ V cm^{-1}, $f=15$ Hz. b) Separation of λ-DNA/Hind III digests using 900 nm and 330 nm silica beads ($E_1=84$ V cm^{-1}, $f=5$ Hz).

shortening the relaxation time that scales with the molecular size N as $\tau \sim N^2$.[31,32]

Figure 4b demonstrates the impact of pore size on the angular separation in which separation between smaller fragments of λ-DNA/Hind III digests was obtained by decreasing bead size from 900 to 330 nm. The resolution improvement can be ascribed to the physical confinement, which profoundly affects DNA stretching and relaxation.[31,32] Tighter confinement can improve electrophoretic stretching and slow down the relaxation of confined DNA molecules.[30] Crystalline arrays offers direct control of pore size (equivalent to ca. 15% the bead size) to adjust the separation power for DNA species of interest. Such flexibility is especially desirable for the applications, such as sequencing single-stranded DNA,[28] which is performed on a length scale still challenging for conventional nanofabrication techniques to access.

In conclusion, we have demonstrated a general microfluidic approach for patterning large-scale colloidal nanoarrays into microdevices, which presents two major merits: first, the use of multiple evaporation microchannels avoids the formation of drying-induced cracks during colloidal crystallization; second, the method features simple microfabrication, fast colloidal deposition, and extremely low cost. Using the technique, we fabricated a 2D microsystem for high-throughput separation of 2–50 kbp DNA. Our studies on the effects of pulsed electric field and pore size present a clear guidance for choosing proper field conditions to sort DNA samples of interest.

Received: February 19, 2008
Revised: April 30, 2008
Published online: July 15, 2008

Keywords: colloidal self assembly · DNA · high-throughput separation · microfluidics · nanofabrication

[1] G. M. Whitesides, B. Grzybowski, *Science* **2002**, *295*, 2418.
[2] Y. N. Xia, B. Gates, Y. D. Yin, Y. Lu, *Adv. Mater.* **2000**, *12*, 693.
[3] R. Mezzenga, J. Ruokolainen, G. H. Fredrickson, E. J. Kramer, D. Moses, A. J. Heeger, O. Ikkala, *Science* **2003**, *299*, 1872.
[4] Y. A. Vlasov, X. Z. Bo, J. C. Sturm, D. J. Norris, *Nature* **2001**, *414*, 289.
[5] M. Ben-Moshe, V. L. Alexeev, S. A. Asher, *Anal. Chem.* **2006**, *78*, 5149.
[6] S. P. Zheng, E. Ross, M. A. Legg, M. J. Wirth, *J. Am. Chem. Soc.* **2006**, *128*, 9016.
[7] Y. Zeng, D. J. Harrison, *Anal. Chem.* **2007**, *79*, 2289.
[8] D. Nykypanchuk, H. H. Strey, D. A. Hoagland, *Science* **2002**, *297*, 987.
[9] L. Meistermann, B. Tinland, *Phys. Rev. E* **2000**, *62*, 4014.
[10] Y. Zeng, D. J. Harrison, *Electrophoresis* **2006**, *27*, 3747.
[11] C. J. Jin, M. A. McLachlan, D. W. McComb, R. M. De La Rue, N. P. Johnson, *Nano Lett.* **2005**, *5*, 2646.
[12] S. Wong, V. Kitaev, G. A. Ozin, *J. Am. Chem. Soc.* **2003**, *125*, 15589.
[13] J. Y. Shiu, C. W. Kuo, P. L. Chen, *J. Am. Chem. Soc.* **2004**, *126*, 8096.
[14] B. T. Mayers, B. Gates, Y. N. Xia, *Adv. Mater.* **2000**, *12*, 1629.
[15] S. M. Yang, H. Miguez, G. A. Ozin, *Adv. Funct. Mater.* **2002**, *12*, 425.
[16] R. C. Hayward, D. A. Saville, I. A. Aksay, *Nature* **2000**, *404*, 56.
[17] Y. Masuda, T. Itoh, K. Koumoto, *Langmuir* **2005**, *21*, 4478.
[18] J. Han, H. G. Craighead, *Science* **2000**, *288*, 1026.
[19] L. R. Huang, J. O. Tegenfeldt, J. J. Kraeft, J. C. Sturm, R. H. Austin, E. C. Cox, *Nat. Biotechnol.* **2002**, *20*, 1048.
[20] L. R. Huang, E. C. Cox, R. H. Austin, J. C. Sturm, *Science* **2004**, *304*, 987.
[21] J. P. Fu, R. B. Schoch, A. L. Stevens, S. R. Tannenbaum, J. Y. Han, *Nat. Nanotechnol.* **2007**, *2*, 121.
[22] E. R. Dufresne, E. I. Corwin, N. A. Greenblatt, J. Ashmore, D. Y. Wang, A. D. Dinsmore, J. X. Cheng, X. S. Xie, J. W. Hutchinson, D. A. Weitz, *Phys. Rev. Lett.* **2003**, *91*, 224501.
[23] C. Allain, L. Limat, *Phys. Rev. Lett.* **1995**, *74*, 2981.
[24] W. P. Lee, A. F. Routh, *Langmuir* **2004**, *20*, 9885.
[25] H. L. Li, W. T. Dong, H. J. Bongard, F. Marlow, *J. Phys. Chem. B* **2005**, *109*, 9939.
[26] L. R. Huang, J. O. Tegenfeldt, J. J. Kraeft, J. C. Sturm, R. H. Austin, E. C. Cox, *Tech. Dig. Int. Electron Devices Meet.* **2002**, 363.
[27] J. L. Viovy, *Electrophoresis* **1989**, *10*, 429.
[28] T. A. J. Duke, R. H. Austin, E. C. Cox, S. S. Chan, *Electrophoresis* **1996**, *17*, 1075.
[29] J. F. Marko, E. D. Siggia, *Macromolecules* **1995**, *28*, 8759.
[30] O. B. Bakajin, T. A. J. Duke, C. F. Chou, S. S. Chan, R. H. Austin, E. C. Cox, *Phys. Rev. Lett.* **1998**, *80*, 2737.
[31] W. Reisner, K. J. Morton, R. Riehn, Y. M. Wang, Z. N. Yu, M. Rosen, J. C. Sturm, S. Y. Chou, E. Frey, R. H. Austin, *Phys. Rev. Lett.* **2005**, *94*, 196101.
[32] J. O. Tegenfeldt, C. Prinz, H. Cao, S. Chou, W. W. Reisner, R. Riehn, Y. M. Wang, E. C. Cox, J. C. Sturm, P. Silberzan, R. H. Austin, *Proc. Natl. Acad. Sci. USA* **2004**, *101*, 10979.

